

AperTO - Archivio Istituzionale Open Access dell'Università di Torino

## Engineering Codrug Solid Forms: Mechanochemical Synthesis of an Indomethacin-Caffeine System

**This is a pre print version of the following article:**

*Original Citation:*

*Availability:*

This version is available <http://hdl.handle.net/2318/1657271> since 2018-01-12T15:24:21Z

*Published version:*

DOI:10.1021/acs.cgd.7b00748

*Terms of use:*

Open Access

Anyone can freely access the full text of works made available as "Open Access". Works made available under a Creative Commons license can be used according to the terms and conditions of said license. Use of all other works requires consent of the right holder (author or publisher) if not exempted from copyright protection by the applicable law.

(Article begins on next page)

# Engineering co-drug solid forms: the mechanochemical synthesis of an indomethacin- caffeine system

*Simone Bordignon,<sup>1</sup> Paolo Cerreia Vioglio,<sup>1†</sup> Emanuele Priola,<sup>1</sup> Dario Voinovich,<sup>2</sup> Roberto Gobetto<sup>1\*</sup>, Yusuke Nishiyama<sup>3</sup> and Michele R. Chierotti<sup>1\*</sup>*

<sup>1</sup>Department of Chemistry and NIS Centre, University of Torino, Via P. Giuria 7, 10125, Torino, Italy

<sup>2</sup>Department of Chemical and Pharmaceutical Sciences, University of Trieste, P.le Europa 1, 34127, Trieste, Italy

<sup>3</sup>JEOL RESONANCE Inc., 3-1-2 Musashino, Akishima, Tokyo 196-8558, Japan

KEYWORDS caffeine, indomethacin, cocrystal, co-drug, Difmetré, dissolution kinetic tests, supramolecular chemistry, crystal engineering, hydrogen bonding, SSNMR, DKT

ABSTRACT This article reports on the preparation and solid-state characterization of an indomethacin-caffeine drug-drug cocrystal (or co-drug) in a 1:1 stoichiometry. These two active ingredients are frequently co-administered as part of a therapy against strong migraines, in a

commercially available fixed dose combination formulation. The X-ray crystal structure of the co-drug is characterized by a hydrogen bond interaction between the carboxylic moiety of indomethacin and the purinic nitrogen atom of caffeine. The combination of multinuclear and multidimensional solid-state NMR measurements ( $^1\text{H}$  MAS,  $^{13}\text{C}$  and  $^{15}\text{N}$  CPMAS,  $^1\text{H}$  DQ MAS,  $^{13}\text{C}$ - $^1\text{H}$  HETCOR,  $^{14}\text{N}$ - $^1\text{H}$  J- and D-HMQC), as well as IR data, provided spectroscopic evidence about the hydrogen atom position along the hydrogen bond axis, thereby confirming the neutral nature of the cocrystal. Furthermore, dissolution kinetic tests revealed superior bioavailability of indomethacin in the co-drug compared to indomethacin alone and to an indomethacin-caffeine physical mixture. On the other hand, the melting point of indomethacin was slightly lower in the cocrystal rather than in the pure drug.

## **Introduction**

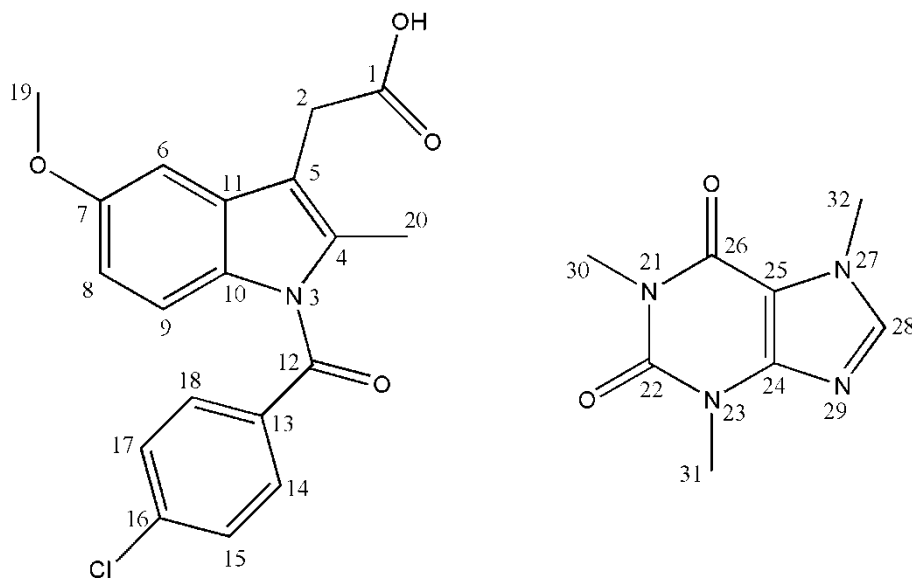
Nowadays, the exploration and synthesis of novel crystal forms is a well-established strategy for tuning physicochemical properties of a certain molecule while preserving its inherent activity.<sup>1</sup> Many papers are devoted to the controlled achievement of new polymorphs,<sup>2</sup> hydrates/solvates,<sup>3</sup> cocrystals<sup>4</sup> and salts<sup>5</sup> with improved performances ranging from pharmaceutical to thermal and optical.<sup>6</sup> A particular type of crystal form is represented by pharmaceutical cocrystals where at least one component is an Active Pharmaceutical Ingredient (API).<sup>7</sup> If both co-formers are APIs, a co-drug, or drug-drug cocrystal, is formed. This is a convenient approach when the two APIs are used in combination to treat a specific disease. Hence, the main purpose of drug-drug cocrystallization is not only to modulate the physicochemical properties of the involved APIs, but also the possibility of taking a single medicine instead of two. This results in reducing the pill burden and also minimizing any

possible mistake by patients, which often lead to higher risks. Indeed, when the necessity of administering more than one drug arises, which is frequent for prolonged and elaborate therapies, complicated schedules for assumptions and doses are involved. It has been calculated that the consequences of a wrong approach to pharmacotherapies have an approximate cost of \$100 billion per year, due to increased hospitalizations and deaths.<sup>8</sup> Further advantages that are not shared with a tablet containing the two individual drugs are the potential improvement of the performances of the cocrystal components and the possibility of patenting the co-drug, which is significantly appealing for pharmaceutical companies from the intellectual property protection point-of-view. Furthermore, the recent approval by the US Food and Drug Administration (FDA) of the first drug-drug cocrystal product may spark even more interest in exploring new drug-drug cocrystal combinations.<sup>9,10</sup>

The rational design of a co-drug reveals to be more challenging than that of a pharmaceutical cocrystal: indeed, the starting materials are thoroughly selected among the APIs that are co-administered in a specific therapy rather than being chosen on the basis of crystal engineering strategies. The investigation of whether a specific supramolecular synthon will occur becomes secondary, but crystal engineering can still offer some helpful insights into the design of co-drugs as well. Several co-drugs can be found in the literature,<sup>11</sup> although they are quite scarce in number due to the complexity in their design and achievement. Some notable examples are theophylline with 5-fluorouracil<sup>12</sup> or barbital,<sup>13</sup> sulfamethazine with theophylline,<sup>14</sup> ethenzamide with gentisic acid<sup>15</sup> and a 1:1 adduct of the anti-HIV drugs lamivudine and zidovudine. The latter, according to screening tests, exhibits better mechanical properties than the starting materials and an improved bulk density in comparison with a physical mixture of the two

components, suggesting that sometimes drug-drug cocrystallization may represent also a strategy to tune the performances of APIs.<sup>16</sup>

Here, we report on the mechanochemical synthesis and solid-state characterization of a 1:1 indomethacin-caffeine (IND·CAFF) co-drug.



**Scheme 1.** Molecular structure of (left) IND and (right) CAFF, with atom numeration.

IND (Scheme 1) is a synthetic non-steroidal anti-inflammatory drug (NSAID) employed in therapies aimed at the treatment of severe migraines,<sup>17</sup> Bartter syndrome,<sup>18</sup> pericarditis<sup>19</sup> and patent ductus arteriosus.<sup>20</sup> Two main polymorphic phases of IND are known, namely  $\alpha$  phase and  $\gamma$  phase, both characterized by a COOH dimeric homosynthon.<sup>21</sup> IND has often been selected as the main API of many cocrystals found in literature:<sup>22-24</sup> for example, cocrystals of IND with saccharine and with nicotinamide have been extensively investigated to examine their structure and biological effects.<sup>25,26</sup> Notably, two drug-drug cocrystals involving IND are already known, namely IND-carbamazepine<sup>27</sup> and IND-lidocaine.<sup>28</sup> CAFF was chosen as a co-former because it can be found together with IND, owing to their synergic effects,<sup>29</sup> in Difmetré® a pharmaceutical containing IND, CAFF and prochlorperazine dimaleate in a molar ratio

1:5.6:0.07. Difenhydramine® can be administered as a film-coated or effervescent tablet or as a suppository and is currently used to treat strong migraines, especially hypnic headaches. Moreover, CAFF possesses a purinic nitrogen moiety (Scheme 1), which, from the crystal engineering point-of-view, is favored in establishing a HB with the carboxylic group of IND. This represents also a promising strategy to improve the bioavailability of IND, since this drug belongs to class II of the Biopharmaceutical Classification System (BCS), because of its low solubility and high permeability.

In this work, several complementary solid-state techniques such as powder and single-crystal X-ray diffraction (PXRD and SCXRD), solid-state NMR (SSNMR), vibrational spectroscopy (Raman and ATR-IR) and calorimetric analyses (DSC and TGA) were combined together to give a full and consistent description of the obtained IND·CAFF drug-drug cocrystal. Both common and advanced SSNMR techniques ( $^1\text{H}$  MAS,  $^{13}\text{C}$  and  $^{15}\text{N}$  CPMAS,  $^1\text{H}$  DQ MAS,  $^{13}\text{C}$ - $^1\text{H}$  HETCOR,  $^{14}\text{N}$ - $^1\text{H}$  J- and D-HMQC) were instrumental in defining the neutral rather than the ionic nature of the adduct, i.e. the position of the hydrogen atom along the observed  $\text{O}\cdots\text{H}\cdots\text{N}$  interaction, supporting the X-ray data. SSNMR was also functional to detect the crystal form present in Difenhydramine® (film-coated tablet). In this regard, and especially for pharmaceutical solids, we note that SSNMR is well suited to investigate the intermolecular interactions that dictate crystal packing, such as hydrogen bonding (HB) and  $\pi$ -stacking, in both pure form and in formulations.<sup>30-33</sup> More importantly, SSNMR has long been used to elucidate the crystal packing interactions in polymorphs<sup>34-36</sup> and cocrystals of IND.<sup>37,38</sup>

The solubility properties were assessed by dissolution kinetic tests, which allowed to evaluate the variation of the solubility rate (i.e. of the bioavailability)<sup>39</sup> of IND in the co-drug with respect

to the pure form and to a heterogeneous mixture of the two drugs in the same ratio as found in Difmetré®.

### **Experimental part**

IND, CAFF and ethyl acetate were purchased from Sigma Aldrich, Zentek and Carlo Erba Reagents, respectively and used without further purification. IND was verified to be in its  $\gamma$  form by PXRD analysis (CSD Refcode: INDMET,<sup>40</sup> Figure S1 in the Supporting Information). Although the supplier declared CAFF batch to be  $\alpha$  form, its experimental PXRD pattern was accounted for by the  $\beta$  form instead (CSD Refcode: NIWFEE03,<sup>41</sup> see Figure S2 in the Supporting Information).

IND·CAFF adduct in the form of a light brown microcrystalline powder was quantitatively obtained by kneading 255 mg (0.7 mmol) of IND and 140 mg (0.7 mmol) of CAFF for 60 minutes at 70 rpm in a ball mill (Retsch AS200 Basic, equipped with a 10 cm diameter basin and a 5 cm diameter steel ball) with 10 drops of ethyl acetate. Yellow crystals suitable for SCXRD were obtained by slow evaporation of a 1:1 IND·CAFF solution in ethyl acetate at room temperature, after addition of crystalline seeds retrieved from the ball-milled microcrystalline powder.

The crystallographic data for IND·CAFF (1:1) have been deposited within the Cambridge Crystallographic Data Centre as supplementary publications under the CCDC number 1544702. This information can be obtained free of charge from the Cambridge Crystallographic Data Centre via [www.ccdc.cam.ac.uk/data\\_request/cifcode](http://www.ccdc.cam.ac.uk/data_request/cifcode) CCDC.

### *X-ray diffraction*

IND·CAFF single crystals were analyzed with a Gemini R Ultra diffractometer operating at 293(2) K, using a Mo-K $\alpha$  source ( $\lambda = 0.71073 \text{ \AA}$ ). Data collection and reduction were performed using the CrysAlisPro software. The crystal structure was solved by direct methods and refined with the full matrix least square technique on  $F^2$  using the SHELXS-97 and SHELXL-97 programs. All non-hydrogen atoms were refined anisotropically; hydrogen atoms were placed in geometrical positions and refined using the riding model. See Table 1 and Table S1 in the Supporting Information for the crystallographic data (refer to Figure S3 for atom numeration).

Powder diffractograms were obtained on a Philips X'Pert PW3020 Bragg-Brentano instrument, equipped with an X-ray source using Cu-K $\alpha$  radiation ( $\lambda = 1.54506 \text{ \AA}$ ) operating at 40 kV and 20 mA. Measurements were carried out in  $\theta/2\theta$  mode, with a scanning range of 3–50° for  $2\theta$ . A comparison among PXRD diffractograms of IND·CAFF,  $\gamma$ -IND and CAFF is reported in the Supporting Information (Figure S4).

**Table 1.** IND·CAFF crystal data.

<b>Crystal data</b>	
Chemical formula	C <sub>19</sub> H <sub>16</sub> ClNO <sub>4</sub> ·C <sub>8</sub> H <sub>10</sub> N <sub>4</sub> O <sub>2</sub>
$M_r$	551.98
Crystal system, space group	Monoclinic, $P2_1/c$
Temperature (K)	293
$a, b, c$ (Å)	14.3110 (5), 14.6343 (4), 12.1818 (4)
$\beta$ (°)	98.298 (3)
$V$ (Å <sup>3</sup> )	2524.54 (14)
$Z$	4
Radiation type	Mo $K\alpha$
$\mu$ (mm <sup>-1</sup> )	0.21
Crystal size (mm)	0.4 × 0.35 × 0.2
$T_{\min}, T_{\max}$	0.765, 1.000
No. of measured, independent and observed [ $I > 2\sigma(I)$ ] reflections	35378, 4614, 3913
$R_{\text{int}}$	0.055
$R[F^2 > 2\sigma(F^2)], wR(F^2), S$	0.046, 0.123, 1.05
No. of reflections, parameters and restraints	4614, 358, 0
$\Delta\rho_{\max}, \Delta\rho_{\min}$ (e Å <sup>-3</sup> )	0.33, -0.23



### *Solid-state NMR measurements*

$^1\text{H}$  MAS,  $^1\text{H}$  DQMAS,  $^{13}\text{C}$ - $^1\text{H}$  HETCOR (indirect detection), and  $^{14}\text{N}$ - $^1\text{H}$  J- and D-HMQC spectra were collected on a Jeol ECZR 600 instrument, operating at a frequency of 600.13, 150.91, and 43.37 MHz for  $^1\text{H}$ ,  $^{13}\text{C}$ , and  $^{14}\text{N}$ , respectively. Samples were packed in 1 mm (o.d.) cylindrical zirconia rotors (sample volume 0.8  $\mu\text{l}$ ). All measurements were acquired at probe temperature with a spinning speed of 70 kHz.  $^1\text{H}$  MAS spectra were performed with an echo pulse sequence ( $90^\circ$ - $\tau$ - $180^\circ$ - $\tau$ ) to remove the probe background ( $^1\text{H}$   $90^\circ$  pulse = 0.77  $\mu\text{s}$ ; 3 transients for all samples). The 2D  $^1\text{H}$  DQ MAS experiments were performed with the back-to-back (BABA)-xy16 recoupling pulse sequence<sup>42</sup> with excitation time durations of eight rotor periods ( $^1\text{H}$   $90^\circ$  = 0.45  $\mu\text{s}$ ; 12 scans;  $t_1$  increments = 128;  $t_{\text{exc}} = t_{\text{rec}} = 114$   $\mu\text{s}$ ; relaxation delay = 18 s). The  $^{13}\text{C}$ - $^1\text{H}$  HETCOR experiments were measured according to the indirect detection method described in detail in earlier studies.<sup>43</sup> In short, the experiment is composed by four parts: 1) a  $^1\text{H}$ - $^{13}\text{C}$  RAMP-CP ( $^1\text{H}$   $90^\circ$  = 0.77  $\mu\text{s}$ ; contact time 1 = 3.5 ms); 2) a  $t_1$  period during which  $^{13}\text{C}$  magnetization evolves in the presence of heteronuclear  $^1\text{H}$  decoupling (TPPM,<sup>44</sup> rf field = 32.5 kHz); 3) the  $^{13}\text{C}$  magnetization is stored along the z-axis ( $^{13}\text{C}$   $90^\circ$  = 0.86  $\mu\text{s}$ ), while the  $^1\text{H}$  magnetization remaining after the first CP transfer is cancelled by reintroducing the  $^1\text{H}$ - $^1\text{H}$  dipolar interactions with a  $^1\text{H}$  irradiation following the homonuclear Rotary Resonance Recoupling ( $R^3$  with  $n = 1/2$ : HORROR) with two  $x$  and  $y$  phases;<sup>45,46</sup> 4) the  $^1\text{H}$  magnetization is detected following the final  $^{13}\text{C}$ - $^1\text{H}$  RAMP-CP transfer (contact time 2 = 0.5 ms), this time under heteronuclear  $^{13}\text{C}$  WALTZ decoupling (rf field 10.5 kHz). In the J- and D-HMQC experiments,  $^1\text{H}$  and  $^{14}\text{N}$   $90^\circ$  pulses were set to 0.77 and 5  $\mu\text{s}$ , respectively. Relaxation delay of 18 s with rotor-synchronization of the  $t_1$  increment,  $\Delta t_1 = 1/v_r$  (14.3  $\mu\text{s}$ ), were employed. 4 transients were

averaged for 16  $t_1$  experiments.  $t_{\text{exc}}$  and  $t_{\text{rec}}$  of 0.43 ms were used for the D-versions. In the D-HMQC experiment, an SR4 pulse sequence was adopted to recouple the dipolar interaction between  $^1\text{H}$  and  $^{14}\text{N}$ .  $^{13}\text{C}$  CPMAS and  $^{15}\text{N}$  CPMAS SSNMR spectra were collected on a Bruker Avance II 400 Ultra Shield instrument, working at 400.23, 100.63, and 40.56 MHz for  $^1\text{H}$ ,  $^{13}\text{C}$  and  $^{15}\text{N}$ , respectively. Samples were packed in cylindrical zirconia rotors (4 mm o.d.), with a sample volume of 80  $\mu\text{l}$ .  $^{13}\text{C}$  and  $^{15}\text{N}$  spectra were acquired at room temperature with a rotation frequency of 12 and 9 kHz, respectively. All  $^{13}\text{C}$  and  $^{15}\text{N}$  experiments employed the RAMP-CP pulse sequence ( $^1\text{H}$   $90^\circ$  pulse = 3.6  $\mu\text{s}$ ; contact time = 4 ms) with the TPPM  $^1\text{H}$  decoupling (rf field = 69.4 kHz) during the acquisition period. Detailed acquisition parameters (number of scans, relaxation delays, contact times) may be found in the Supporting Information (Table S2).  $^1\text{H}$ ,  $^{13}\text{C}$ ,  $^{14}\text{N}$  and  $^{15}\text{N}$  chemical shift scales were referenced with the resonance of adamantane ( $^1\text{H}$  signal at 1.87 ppm), glycine ( $^{13}\text{C}$  methylene signal at 43.5 ppm),  $(\text{NH}_4)_2\text{SO}_4$  ( $^{14}\text{N}$  signal at 0 ppm and  $^{15}\text{N}$  signal at 24.6 ppm with respect to  $\text{NH}_3$ ), respectively as external standards.

#### *Thermal analysis*

DSC curves were collected on a DSC Q200 TA Instrument. Samples were accurately weighted (5–10 mg) and put into sealed aluminum pans. Calibration for temperature and heat flow was performed using a high purity standard of indium. All measurements were performed in a 40–350  $^\circ\text{C}$  temperature range, with heating/cooling rates of  $10^\circ\text{C}\cdot\text{min}^{-1}$ . TGA measurements were performed over a temperature range of 40–400 $^\circ\text{C}$  under a  $50\text{ ml}\cdot\text{min}^{-1}$   $\text{N}_2$  flow, on a Q600 SDT TA instrument equipped with a DSC heat flow analyzer. Samples (5–10 mg of weight) were placed into the furnace inside alumina crucibles and heated with a ramp of  $10^\circ\text{C}\cdot\text{min}^{-1}$ .

#### *Dissolution kinetic tests (DKT)*

DKT tests were carried out in phosphate buffer (pH = 7.4). For each measurement, 5 mg of IND either pure or as IND·CAFF or as a physical mixture (prepared in the same IND-to-CAFF molar proportions as in the cocrystal) were added to the thermostatically-controlled (at 37°C) dissolution medium (100 ml). Dissolution parameters were evaluated for 60 min. The solution was kept homogeneous by continued stirring at 100 rpm, and concentrations were measured using an optical fiber system (HELLMA, Milan, Italy) linked to a spectrophotometer (ZEISS, Germany). UV measurements were performed at the maximum absorption wavelength of the analyzed molecule (318 nm for IND).

#### *IR and FT-Raman spectroscopy*

Raman spectra were collected on a Bruker Vertex 70 instrument, equipped with a RAM II module. The employed excitation source was a 1064 nm laser with a power varying in the range 10-50 mW, and a number of scans between 80 and 1000, depending on the sample; resolution was set at 4 cm<sup>-1</sup> for all spectra. A spectral range of 50–4500 cm<sup>-1</sup> was scanned, using a CaF<sub>2</sub> beam splitter. Raman spectra are reported in the Supporting Information, Figures S5 and S6.

IR-ATR spectra were collected on a Fourier transform Equinox 55 (Bruker) spectrophotometer equipped with an ATR device; resolution was set at 2 cm<sup>-1</sup> for all spectra. A spectral range of 400–4000 cm<sup>-1</sup> was scanned, using KBr as a beam splitter. IR-ATR whole spectra are reported and discussed in the Supporting Information, Figure S7.

Both Raman and IR-ATR spectra were processed with Bruker's OPUS Version 7.0 software.

Vibrational spectroscopies were used during the crystal form screening to evaluate the formation of new phases, to assess the presence of COOH/COO<sup>-</sup> bands and to monitor the kinetics of the mechanochemical reaction.

## Results and discussion

IND and CAFF are likely to give a multicomponent crystal form due to the presence of a heterocyclic purinic nitrogen atom (CAFF) and a carboxylic group (IND) which are favored in establishing a  $\text{COOH}\cdots\text{N}_{\text{heterocyclic}}$  supramolecular HB (1597 hits for the same synthon found in a CSD survey, v5.38, Feb 2017). Indeed, seven cocrystals of isoniazid, which contains a heterocyclic nitrogen atom, with mono- and dicarboxylic acids,<sup>47</sup> as well as 2 out of 7 published IND cocrystal structures (CSD Code: LAPPEY,<sup>48</sup> SESKUY<sup>27</sup> and SESKUY01;<sup>49</sup> the last two refer to the same cocrystal, whose structure was solved from PXRD and single crystal, respectively) exhibit the synthon of interest.

Mechanochemical synthesis by kneading procedure revealed to be successful in quantitatively preparing the IND·CAFF co-drug. All analytic techniques, Raman, IR-ATR, PXRD, SSNMR and thermal methods, show the quantitative formation of a new phase through remarkable changes in the spectral features. IR, Raman and SSNMR spectra are discussed in depth in the Supporting Information. SCXRD provided the structure of the co-drug while IR and mainly SSNMR show the positioning of the H atom at the COOH group, i.e. the formation of a cocrystal rather than a salt.

The mechanochemical reaction was monitored by following changes of the IND benzoyl C=O vibration in the Raman spectrum (Figure 1, range 1730-1650  $\text{cm}^{-1}$ ) relying on the sensitivity of the technique to assess the quantitative conversion. Two different cases were examined: grinding in absence (dry grinding) or in presence (kneading) of catalytic amounts of ethyl acetate. In the first case (Figure 1a), the conversion was very slow and not quantitative even after 20 minutes, as implied by the still strong IND band at 1699  $\text{cm}^{-1}$  and by the weak IND·CAFF  $\nu\text{C}=\text{O}$  band at 1677  $\text{cm}^{-1}$ . In the second case (Figure 1b), the conversion was complete after only 3 minutes of

kneading. This is not surprising since it is well known that kneading, besides driving the conversion toward a specific product, is used to speed up the kinetics of mechanochemical reactions.<sup>50</sup>

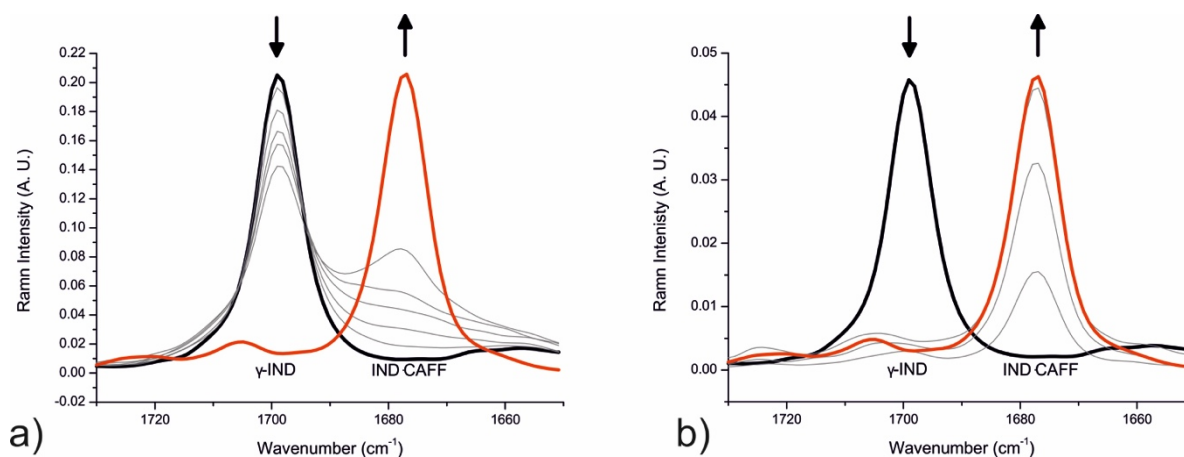


**Figure 1.** Evolution of the IND benzoyl C=O vibration Raman band during the mechanochemical reaction between IND and CAFF. (a) dry grinding with spectra registered every 4 minutes; (b) kneading (ethyl acetate) with spectra acquired with an interval of 1 minute between each other.

#### *X-Ray structure characterization*

SCXRD data afforded a detailed picture of the new formed phase. A comparison of the experimental and calculated PXRD patterns (Figure S8) indicates that the single crystal structure is representative of the bulk. The asymmetric unit displays a single molecule of IND and CAFF, which crystallize in the monoclinic  $P2_1/c$  space group. The structure (Figure 2) presents the expected O-H $\cdots$ N HB interaction between the carboxylic OH of IND and the purinic nitrogen atom of CAFF. The O6 $\cdots$ N29 distance is 2.708(3) Å and represents the shortest contact that occurs in the structure (for the complete atom numeration, refer to Figure S3 in the Supporting Information). The carbon/oxygen distances (C1–O6H= 1.315(2) Å, and (C1=O5) = 1.198(2) Å)

are comparable to those generally observed for a carboxylic moiety, rather than a carboxylate group.<sup>51</sup>

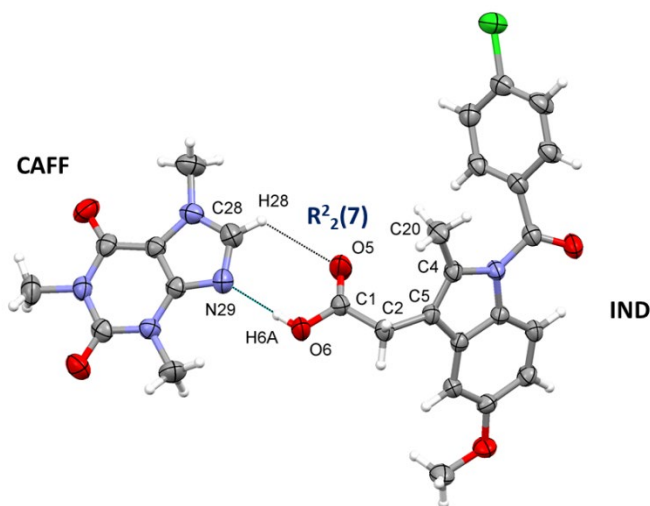


**Figure 2.**  $R^2_2(7)$  HB arrangement of IND and CAFF in IND·CAFF with relevant atom numbering. Thermal ellipsoids drawn at 70% of probability. (C = grey; H = white; O = red; N = azure; Cl = green).

Owing to the uncertainty in the position of the O-H hydrogen atom, further and more reliable insights on the character of the adduct has been provided by IR and SSNMR (see “*Solid-state NMR characterization*” paragraph below). The carbonyl region of the IR spectrum of IND·CAFF (Figure 3) does not present shifts attributable to the formation of a  $\text{COO}^-$  in the  $\nu(\text{C}=\text{O})$  bands. The shifts are indeed in the order of  $10\text{ cm}^{-1}$ , while salification implies much larger shifts at lower wave numbers (around  $30\text{-}50\text{ cm}^{-1}$  up to  $100\text{ cm}^{-1}$ ). Moreover, the signal at  $1483\text{ cm}^{-1}$ , which is typically medium-weak for a  $\text{NH}^+$  deformation mode in a salt, appears as a strong peak in the spectrum of IND·CAFF and it is most likely due to a CCH deformation mode; the same can be said about the signal at about  $1235\text{ cm}^{-1}$ , ascribable to an *in-plane* CH deformation. At  $737\text{ cm}^{-1}$  we can observe the typical signal of a COOH *out-of-plane* deformation, while there is

no trace of the characteristic peak at  $1370\text{ cm}^{-1}$ , attributed to the asymmetric stretching of  $\text{COO}^-$  in salts.<sup>52</sup> All this agrees with the presence of a  $\text{COOH}$  group involved in a HB and can be used as preliminary evidence of the formation of a cocrystal instead of a salt, thus confirming the neutral character of the adduct.

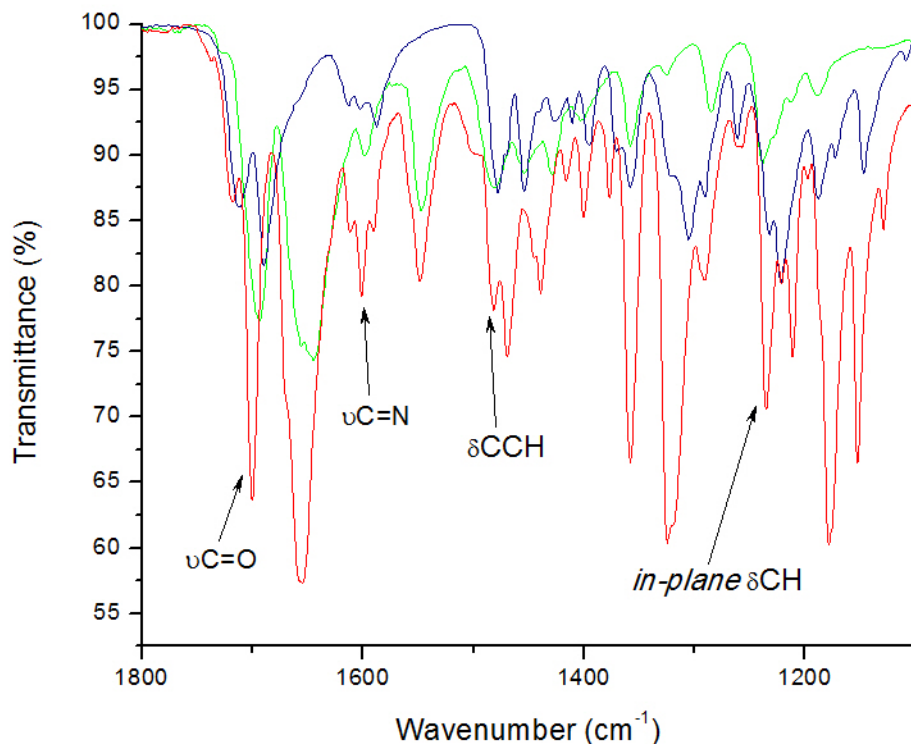


**Figure 3.**  $1800\text{-}1100\text{ cm}^{-1}$  region of the IR-ATR spectra of IND-CAFF (red), IND (blue) and CAFF (green). See Figure S7 in the Supporting Information for the whole spectra.

The  $\text{COOH}_{\text{IND}}\cdots\text{N}_{\text{CAFF}}$  HB drives the self-assembly of the cocrystal components (Figure 4a) through the formation of a  $\text{R}^2_2(7)$  motif. This motif (with  $\text{C}\cdots\text{O}$  distance  $< 3.3\text{ \AA}$ )<sup>53</sup> was observed in more than 180 structures registered in the CSD v5.38 (Feb 2017). The 3D structure of the IND-CAFF dimer depends on the bending of the  $\text{CH}_2\text{COOH}$  group out of the indole plane of

IND due to sterical hindrance between C1 and C20 (or O5 and C20) (torsion angle C1-C2-C5-C4 = 71.4(7)°). On the other hand, a planar arrangement between the COOH group and CAFF is preferred. This leads to a dihedral angle between the indole and CAFF of 65.4(6)°. A detailed analysis of the whole crystal structure revealed that  $\pi$ - $\pi$  stacking interactions<sup>54</sup> between indole and purinic fragments also occur, with a distance between planes of 3.536(4) Å (intercentroid distance) and an interplanar angle of 13.4(2)°. These interactions contribute to form the ribbon-like assemblies depicted in Figure 4b; each CAFF molecule is thus stacked to an IND molecule, which is in turn H-bonded to another CAFF molecule.

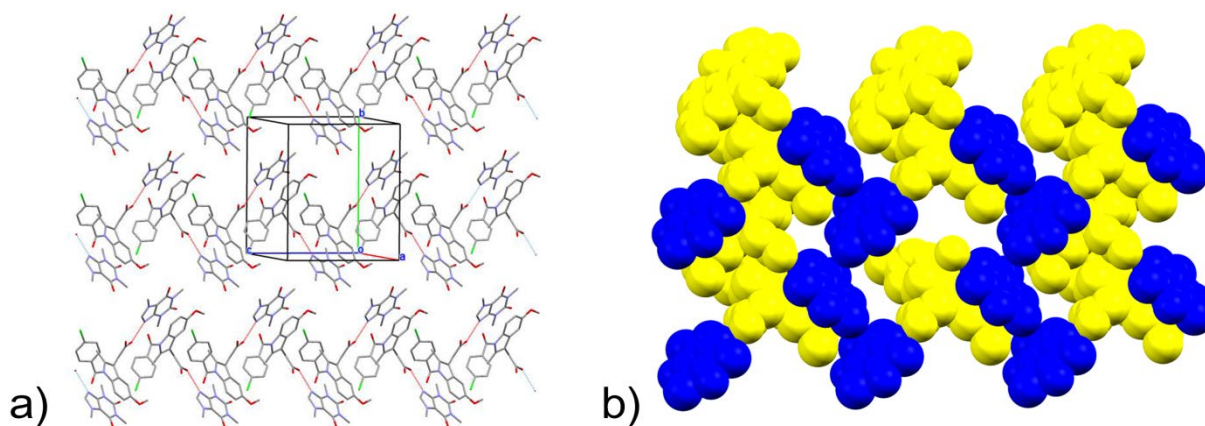


**Figure 4.** Perspective views of the IND-CAFF drug-drug cocrystal: (a) packing diagram highlighting the HB framework (blue and red dots); (b) spacefill model excerpt of crystal packing, in which ribbons of IND (yellow) alternate with CAFF molecules (blue).

#### *Solid-state NMR characterization*

SSNMR has long proven to be highly complementary to X-ray diffraction to detect and characterize the HB in supramolecular materials thanks to the sensitivity of many NMR parameters to the proton position.<sup>51</sup> In particular, besides providing information about purity,



degree of crystallinity, number of independent molecules, etc., it is fundamental for probing the neutral or ionic nature of the adduct. In our case SSNMR was instrumental to:

- define the position of the hydrogen atom along the O...H...N HB through  $^{13}\text{C}$ ,  $^{15}\text{N}$  CPMAS and  $^{14}\text{N}$ - $^1\text{H}$  J-/D-HMQC experiments which allowed definitive understanding whether the adduct has to be regarded as a cocrystal or a salt;
- explore the different behaviours of the J- and D- versions of the HMQC pulse sequence on the system under study;
- demonstrate its ability in studying complex matrices such as marketed tablets, i.e. Difmetr  ;
- probe the strength and the network of weak interactions by means of  $^1\text{H}$  MAS and  $^1\text{H}$  DQ MAS spectra.<sup>55</sup>

All  $^1\text{H}$ ,  $^{13}\text{C}$  and  $^{15}\text{N}$  chemical shifts and assignments of the IND-CAFF product are reported in Table 2, referring to Scheme 1 for atom numbering. Assignments were aided by the  $^{13}\text{C}$ - $^1\text{H}$  HETCOR experiment (Figure S9 in the Supporting Information) and by previously reported data.<sup>34</sup>

**Table 2.**  $^1\text{H}$ ,  $^{13}\text{C}$  and  $^{15}\text{N}$  chemical shifts (ppm) with assignments of CAFF, IND and IND-CAFF.

$^{13}\text{C}$  assignments were made from the correlations observed in the  $^{13}\text{C}$ - $^1\text{H}$  HETCOR experiment (Figure S9) and from previously reported data.<sup>34</sup>

Atom	Notes	IND	CAFF	IND-CAFF
<b><math>^1\text{H}</math></b>				
	COOH	12.6		13.1
H2	CH <sub>2</sub>	2.2		2.3
H6	CH(Ar)	6.1		6.3
H8	CH(Ar)	6.0		6.2
H9	CH(Ar)	7.2		8.5
H14-18	CH(Ar)	6.1		7.4
H19	O-CH <sub>3</sub>	3.3		3.5

H20	<b>CH<sub>3</sub></b>	2.2		1.8
H28	<b>CH(Ar)</b>		7.6	7.8
H30	<b>N-CH<sub>3</sub></b>		2.3	2.3
H31	<b>N-CH<sub>3</sub></b>		2.3	2.3
H32	<b>N-CH<sub>3</sub></b>		3.2	3.2
<b><sup>13</sup>C</b>				
C1	<b>COOH</b>	179.0		171.8
C2	<b>C-COOH</b>	28.1		26.4
C4	<b>C-CH<sub>3</sub></b>	136.6		135.7
C5	<b>C(Ar)</b>	112.6		110.4
C6	<b>CH(Ar)</b>	97.8		96.0
C7	<b>C(Ar)-O</b>	156.6		154.1
C8	<b>CH(Ar)</b>	112.6		113.5
C9	<b>CH(Ar)</b>	115.6		116.8
C10-11	<b>C(Ar)</b>	131.0		129.5
C12	<b>C=O</b>	167.6		167.2
C13	<b>C(Ar)</b>	134.4		135.7
C14	<b>CH(Ar)</b>	131.9		129.5
C15	<b>CH(Ar)</b>	126.9		129.5
C16	<b>C(Ar)-Cl</b>	141.5		142.8
C17	<b>CH(Ar)</b>	126.9		129.5
C18	<b>CH(Ar)</b>	131.9		129.5
C19	<b>O-CH<sub>3</sub></b>	55.1		56.1
C20	<b>CH<sub>3</sub></b>	13.5		18.2
C22	<b>C=O</b>		148.6	145.0
C24	<b>C(Ar)</b>		151.2	151.1
C25	<b>C(Ar)</b>		106.2	106.7
C26	<b>C=O</b>		154.6	155.4
C28	<b>CH(Ar)</b>		142.8	142.8
C30-31	<b>N-CH<sub>3</sub></b>		31.0	28.9
C32	<b>N-CH<sub>3</sub></b>		35.4	33.1
<b><sup>15</sup>N</b>				
N3	<b>N-C=O</b>	173.6		175.3
N21	<b>N-CH<sub>3</sub></b>		150.1	150.2
N23	<b>N-CH<sub>3</sub></b>		115.2	112.2
N27	<b>N-CH<sub>3</sub></b>		158.0	158.8
N29	<b>N=C</b>		230.0	213.0

The neutral nature of IND·CAFF has been confirmed by the  $^{13}\text{C}$  signal at 171.8 ppm (Figure 5), which is in the range of typical chemical shift values of carboxylic groups involved in a HB interaction; likewise, the small low-frequency shift of the  $^{15}\text{N}$  purinic resonance (Figure 6), which ranges from 230.0 ppm in pure CAFF to 213.0 ppm in IND·CAFF, is symptomatic of the formation of a HB without proton transfer.<sup>51,55</sup> Further details on the  $^{13}\text{C}$  and  $^{15}\text{N}$  CPMAS spectra are reported in the Supporting Information.

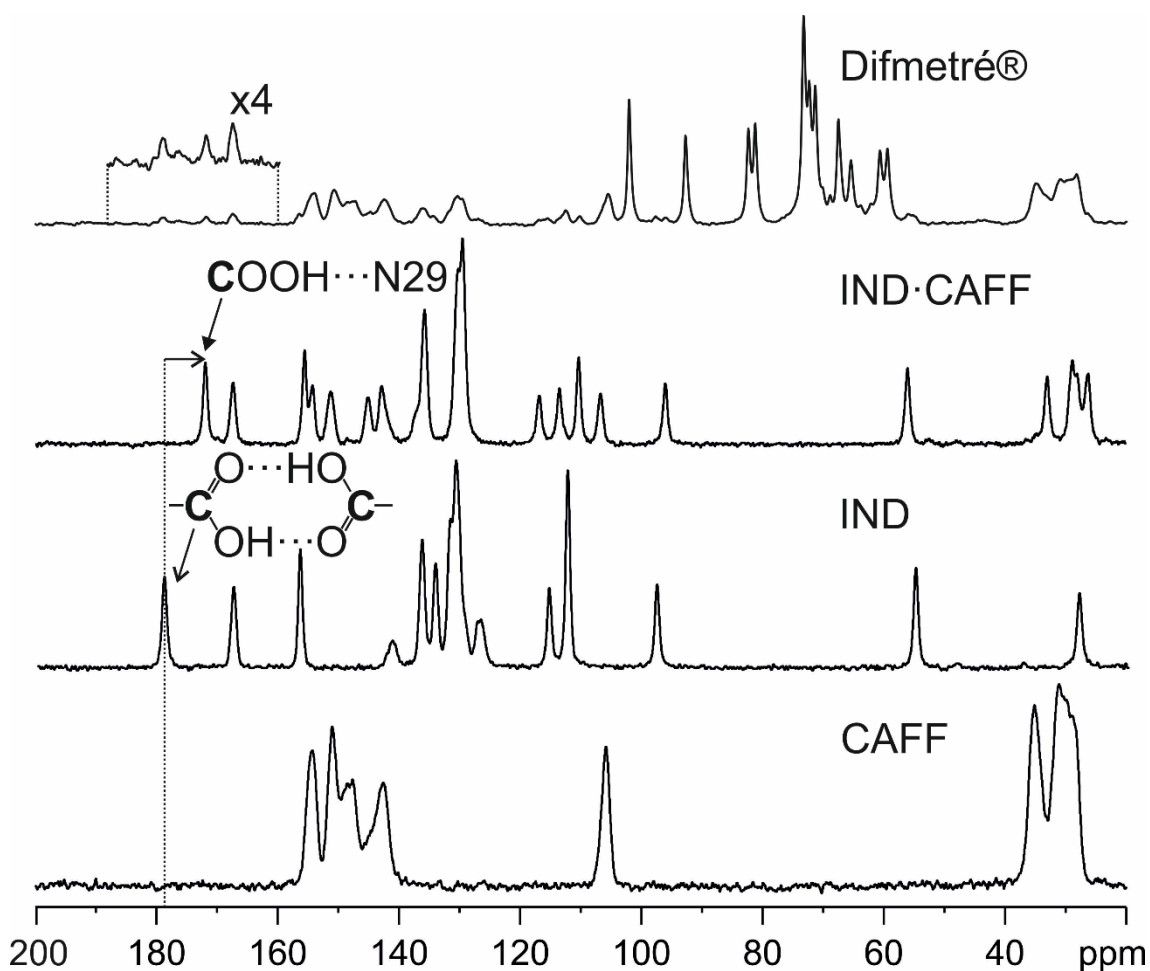


**Figure 5.**  $^{13}\text{C}$  (100.63 MHz) CPMAS spectra with relevant assignments of CAFF, IND, IND·CAFF and film-coated Difmetré® tablet, acquired with a spinning speed of 12 kHz at room temperature.

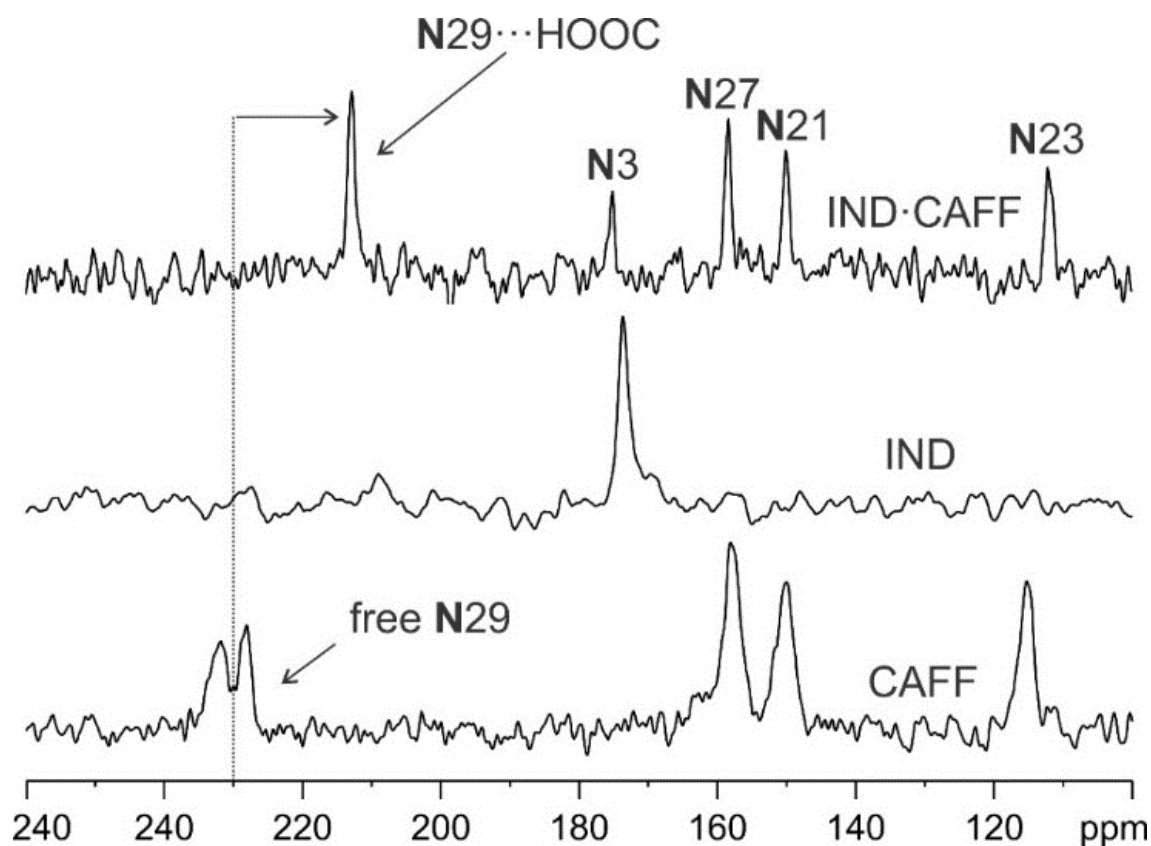


**Figure 6.**  $^{15}\text{N}$  (40.56 MHz) CPMAS spectra with assignments of CAFF, IND, and IND·CAFF, acquired with a spinning speed of 9 kHz at room temperature.

The lack of any significant correlation in the rotor-synchronized  $^{14}\text{N}$ - $^1\text{H}$  J-HMQC experiment (not shown) provides direct evidence of the formation of a  $\text{N}\cdots\text{H}\cdots\text{O}$  rather than a  $\text{N}^+\cdots\text{H}\cdots\text{O}^-$  contact. Indeed, this experiment achieves indirect detection of  $^{14}\text{N}$  lineshapes through a combination of J-coupling and residual dipolar splitting (RDS).<sup>56,57</sup> Thus, the absence of any correlation, independently from the  $\tau_{\text{exc}}$  (see the 1D  $\tau_{\text{exc}}$  optimization data in Figure S10 in the Supporting Information) and considering a  $T_2'$  (3.2 ms) long enough to provide correlation (see Supporting Information for further discussion), implies no  $^1\text{J}_{\text{H-N}}$ -coupling and thus no covalent bond. This also indicates that RDS is not sufficient to transfer significant magnetization to give correlation in  $\text{N}\cdots\text{H}\cdots\text{O}$  systems. On the other hand, the dipolar version (D-HMQC), where the

magnetization transfer is provided by  $^1\text{H}$ - $^{14}\text{N}$  dipolar interaction, shows a signal increasing with longer  $\tau_{\text{exc}}$  (see the 1D  $\tau_{\text{exc}}$  optimization data in Figure S10 in the Supporting Information) in agreement with the long recoupling time needed to transfer magnetization between not directly bonded atoms. The 2D  $^{14}\text{N}$ - $^1\text{H}$  D-HMQC (Figure S11 in the Supporting Information) was useful to probe proximities between not covalently bonded  $^1\text{H}$  and  $^{14}\text{N}$  nuclei. Table S3 in the Supporting Information reports the observed correlations, which agree with the X-ray structure.

A  $^{13}\text{C}$  CPMAS SSNMR analysis was also performed directly on a film-coated Difmetré® tablet, previously ground to be packed in the SSNMR rotor. Interestingly, characteristic signals of pure  $\gamma$ -IND, pure CAFF and IND·CAFF appear in the spectrum (Figure 5, see Supporting Information for full description), suggesting the presence of a small amount of co-drug in the tablet. According to the very little amount present in Difmetré® (about 0.6% w/w), prochlorperazine dimaleate is not visible. To verify whether the co-drug formation was due to the pressure applied for making the tablet, we pressed (10 tons) mixtures of IND and CAFF (1:1) and of IND, CAFF and mannitol (1:1:7.4; this molar ratio reproduces a similar dilution of the two APIs in Difmetré®) to produce two tablets: in both cases no traces of IND·CAFF were found in the respective Raman spectra (data not shown). It is worth noting that the presence of the co-drug in Difmetré® was not declared and no patents were found. On the other hand, the effervescent tablet does not contain the co-drug as revealed by Raman spectra (see Figure S6 in the Supporting Information).

The  $^1\text{H}$  MAS spectrum (Figure 7) of IND·CAFF is characterized by a resonance at 13.1 ppm associated to the carboxylic proton of IND involved in the  $\text{COOH}\cdots\text{N}29$  interaction.

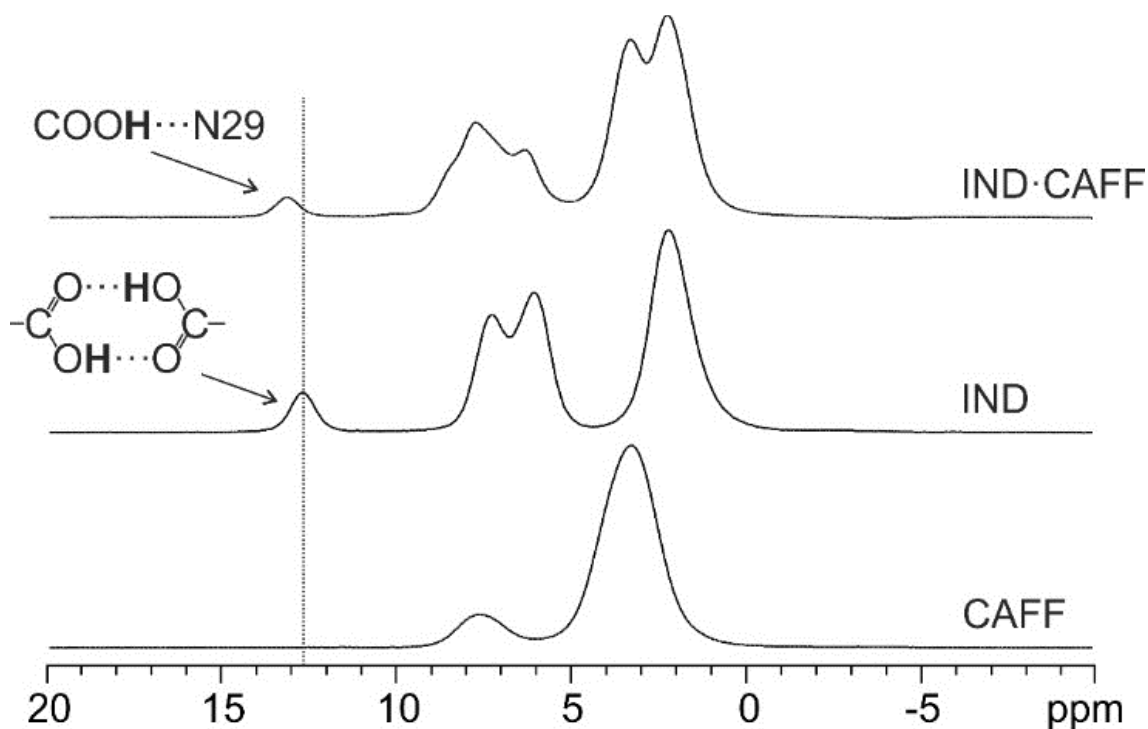


**Figure 7.**  $^1\text{H}$  (600 MHz) MAS spectra with relevant assignments of CAFF, IND, and IND-CAFF, acquired with a spinning speed of 70 kHz at probe temperature.

This signal moves from 12.6 ppm in pure  $\gamma$ -IND to 13.1 ppm in the cocrystal, thus indicating a stronger interaction in the co-drug than in the  $\gamma$ -IND alone. Indeed, it is well known that the high-frequency shift due to HB formation is related to the strength of the contact (i.e., the larger the shift, the stronger the HB).<sup>55</sup> These resonances are associated to a COOH dimeric homosynthon O-H...O (O...O = 2.666 Å) and to a O-H...N (O...N = 2.708 Å) HB, respectively. We decided to carry out several two-dimensional experiments in order to refine NMR signals assignments and to further explore the network of intermolecular interactions in the co-drug. Indeed, Sebastiani and co-workers have elegantly demonstrated<sup>58</sup> that solid-state  $^1\text{H}$  chemical shifts are strongly influenced not only by HB geometry but also by packing effects,  $\pi$ -stacking and related phenomena: taking four strongly H-bonded molecular crystals of aminoacids, they

systematically observed the proton chemical shift to move toward high frequencies when including crystal packing effects into periodic first-principles calculations. More recently, Brown and co-workers used  $\gamma$ -IND as a case study<sup>36</sup> to probe the intermolecular interactions framework by  $^1\text{H}$  DQ MAS spectroscopy, thus observing subtle differences in H–H proximities due to crystal packing. In our case, the  $^1\text{H}$  DQ MAS experiment (Figure S12 in the Supporting Information) shows DQ signals at 20.9 and 15.4 ppm, indicating spatial proximities within approximately 3 Å, between the IND's carboxylic proton and both CAFF's H28 and H31 ( $13.1 + 7.8 = 20.9$  ppm and  $13.1 + 2.3 = 15.4$  ppm, respectively) in nice agreement with the SCXRD structure. In particular, the OH-H28 DQ correlation is spectroscopic evidence of the short C–H $\cdots$ O contact observed, which contributes as a driving force for the co-drug formation through a  $\text{R}^2_2(7)$  interaction. Further correlations are listed in Table S4 in the Supporting Information, together with discussion.

#### *Calorimetric measurements*

IND·CAFF was analyzed through DSC and TGA to evaluate its thermal properties, the presence of water or solvents in the crystal lattice, and its purity. By comparing the thermal profiles of the co-drug and the ones of the starting materials, it was possible to quantify the variation in the thermal stability of both CAFF and IND after cocrystallization. A comparison between the DSC and TGA curves of the co-drug and the reagents is shown in Figures S13 and S14, respectively. IND·CAFF does not exhibit traces of water or solvents, nor undergoes any polymorphic transitions up to the melting point (onset T:  $\sim 147^\circ\text{C}$ ; peak T:  $\sim 149^\circ\text{C}$ ). It is notable that IND·CAFF has a lower melting point than CAFF and IND, both measuring about  $161^\circ\text{C}$  (onset T:  $\sim 156^\circ\text{C}$  and  $\sim 159^\circ\text{C}$ , respectively). A similar melting point was observed also for the cocrystal with 2-amino-5-methylpyridinium (onset T:  $\sim 146^\circ\text{C}$ ; peak T:  $\sim 148^\circ\text{C}$ ),<sup>48</sup> while the

cocrystal with saccharine melts at around 184°C.<sup>24</sup> As discussed in the SSNMR results section, this is probably due to the whole set of intermolecular interactions that define the crystal packing and also affects, among other physicochemical properties, the thermal properties of the sample. On the other hand, it is worth noting that only the IND-saccharine cocrystal preserves the COOH dimeric homosynthon typical of all IND polymorphs. At the melting temperature, the co-drug splits into the starting reagents, as the decomposition temperatures are those of pure CAFF (onset T: ~243°C) and  $\gamma$ -IND (onset T: ~286°C) as expected.

#### *Dissolution kinetic tests*

DKT tests were performed to determine in which extent the cocrystallization with CAFF, already soluble in water, changed the dissolution rate of pure  $\gamma$ -IND. Pure IND (blue curve in Figure 8) presents a low dissolution rate, as expected for a compound which is hardly soluble in water. The dissolution profile of pure IND improved slightly in the presence of an equimolar amount of pure CAFF (orange circles in Figure 8); such slight improvement can be related to the presence of CAFF as an additive, well known for its hydrotropic effects.<sup>59</sup> On the other hand, it is possible to see how the dissolution profile of IND (grey circles in Figure 8) in the co-drug exhibits a drastic dissolution improvement if compared to the dissolution profiles of both physical mixture and pure API, reaching very high levels of solubilization (about 30 mg/L) after only one minute.



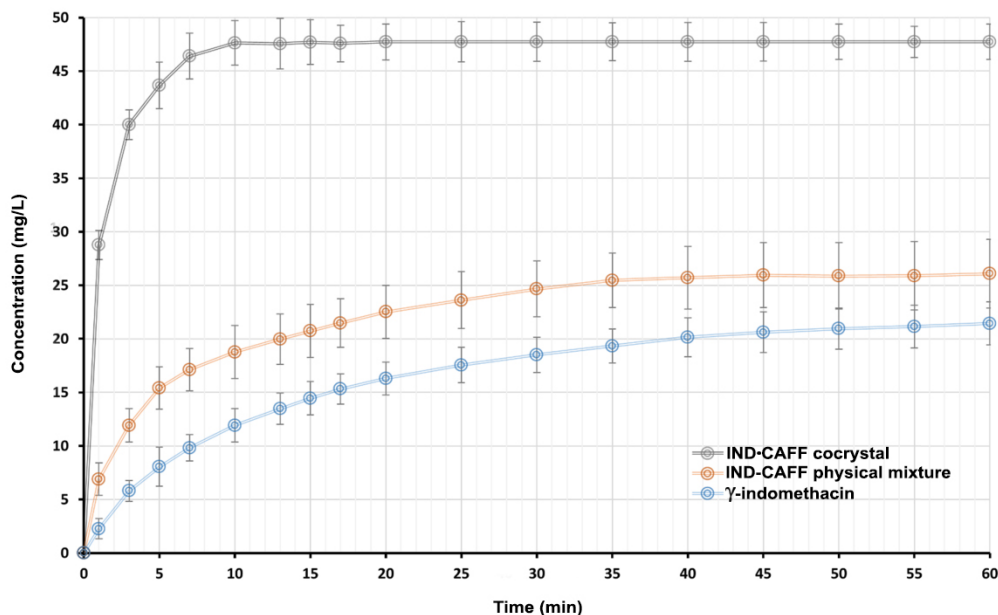


**Figure 8.** Concentration (mg/L) profiles in time (min) for unaltered  $\gamma$ -IND (blue curve), IND-CAFF physical mixture (1:1 ratio) (orange curve) and for IND-CAFF (grey curve).

The AUC (Area Under the Curve) of IND·CAFF, calculated through the trapezoidal rule in the considered range of time, measured 2784 mg\*min/L. This value was then divided by the AUC value of pure IND (1002 mg\*min/L) and that of the corresponding physical mixture (1350 mg\*min/L) to determine the *in vitro* bioequivalence of the samples, obtaining the following values: 2.78 and 2.06, respectively. This means that, although not comparable to the improvement achieved by the IND-saccharine cocrystal,<sup>24</sup> IND·CAFF has an *in vitro* bioavailability 3 times higher than that of the pure drug and double with respect to the simple physical mixture.

## CONCLUSIONS

We demonstrated how simple mechanochemical techniques like grinding were effective in quantitatively producing a new and interesting crystalline co-drug between IND and CAFF.

The X-ray structure of the cocrystal is characterized by a HB between the carboxylic group of IND and the purinic nitrogen of CAFF and exhibits staggered IND-CAFF couples held together also by  $\pi$ - $\pi$  interactions.

Solid-state NMR and IR analyses confirmed the cocrystalline nature of the sample with the formation of a O-H...N HB. Specifically,  $^{13}\text{C}$  and  $^{15}\text{N}$  CPMAS spectra point out there was no protonic transfer from the acid to the base.  $^{14}\text{N}$ - $^1\text{H}$  J- and D-HMQC spectra further proved the carboxylic proton of IND to be covalently bonded to O instead of the purinic nitrogen atom of CAFF. The  $^1\text{H}$  MAS and  $^1\text{H}$  DQ MAS spectra of the samples agreed with the formation of a  $\text{R}^2_2(7)$  HB motif in the cocrystal.

The melting point, determined through DSC analysis, is lower in the co-drug ( $149^\circ\text{C}$ ) than in the starting materials (about  $161^\circ\text{C}$  for both APIs). Finally, solubilization properties of IND were notably improved in the cocrystal with respect to both pure  $\gamma$ -IND (3 times) and IND-CAFF physical mixture (2 times).

Drug-drug cocrystallization proves to be an excellent expedient to take a single medicine instead of more than one while improving the performances of APIs. This results in reducing the risks associated both to a wrong approach to the therapy and to potential side effects of the drug.

#### ASSOCIATED CONTENT

PXRD patterns, Raman spectra, IR-ATR whole spectra, additional SSNMR data and spectra, DSC and TGA graphs, along with further discussion.

## AUTHOR INFORMATION

### Corresponding Authors

\* (M.R.C.) E-mail: michele.chierotti@unito.it. Tel: +39 011 670 7523. \* (R.G.) E-mail: roberto.gobetto@unito.it. Tel: +39 011 670 7520.

### Present Addresses

† Aix-Marseille Université, CNRS, ICR (UMR 7273), 13397 Marseille cedex 20, France.

## ACKNOWLEDGMENTS

S. B. thanks GIDRM and the Annalaura Segre's family for the scholarship "GIDRM/Borse Annalaura Segre". P. C. V. thanks the Istituto Nazionale della Previdenza Sociale (INPS) for a scholarship. The authors are indebted with Jeol Company for helpful technical assistance and cooperation. Elena Amadio is acknowledged for the drawing in the TOC.

## REFERENCES

- (1) Grifasi F.; Chierotti M. R.; Gaglioti K.; Gobetto R.; Maini L.; Braga D.; Dichiarante E.; Curzi M. *Cryst. Growth Des.* **2015**, *15*, 1939–1948.
- (2) Kassuha D. E.; Aiassa V.; Bruno F. P.; Cuadra G.; Sperandeo N. R. *Pharm. Dev. Technol.* **2015**, *20*, 401–409.

- (3) Arora K. K.; Thakral S.; Suryanarayanan R. *Pharm. Res.* **2013**, *30*, 1779–1789.
- (4) Surov A. O.; Solanko K. A.; Bond A. D.; Bauer-Brandl A.; Perlovich G. L. *CrystEngComm* **2016**, *18*, 4818–4829.
- (5) Chi Y.; Liu C.; Ren T.; Wang X.; Yang Q.; Yang Z.; Yang Y.; Yang S.; Gu J.; Hu C. *Cryst. Growth Des.* **2016**, *16*, 3180–3189.
- (6) Mulye S. P.; Jamadar S. A.; Karekar P. S.; Pore Y. V.; Dhawale S. C. *Powder Technology* **2012**, *222*, 131–138.
- (7) Aitipamula S.; Banerjee R.; Bansal A. K.; Biradha K. et al. *Cryst. Growth Des.* **2012**, *12*, 2147–2152.
- (8) Klobusicky, J. J.; Aryasomayajula, A.; Marko N. *AMIA Annu. Symp. Proc.* **2015**, *2015*, 766–774.
- (9) Wang, J.; Yu, Q.; Dai, W.; Mei, X. *Chem. Commun.* **2016**, *52*, 3572–3575.
- (10) Putra O. D.; Yoshida T.; Umeda D.; Higashi K.; Uekusa H.; Yonemochi E. *Cryst. Growth Des.* **2016**, *16*, 5223–5229.
- (11) Thipparaboina, R.; Kumar, D.; Chavan, R. B.; Shastri, N. R. *Drug Discovery Today* **2016**, *21*, 481–490.
- (12) Zaitu, S.; Miwa, Y.; Taga, T. *Acta Crystallogr., Sect. C: Cryst. Struct. Commun.* **1995**, *51*, 1857–1859.
- (13) Nakao, S.; Fujii, S.; Sakaki, T.; Tomita, K. *Acta Crystallogr., Sect. B: Struct. Crystallogr. Cryst. Chem* **1977**, *33*, 1373–1378.

- (14) Lu, J.; Rohani, S. *J. Pharm. Sci.* **2010**, *99*, 4042–4047.
- (15) Aitipamula, S.; Chow, P. S.; Tan, R. B. H. *Acta Crystallogr., Sect. E: Struct. Rep. Online* **2010**, *66*, O1045–O1046.
- (16) Bhatt, P. M.; Azim, Y.; Thakur, T. S.; Desiraju, G. R. *Cryst. Growth Des.* **2009**, *9*, 951–957.
- (17) VanderPluym, J. *Curr. Neurol. Neurosci. Rep.* **2016**, *16*, 5.
- (18) Amsalem, H.; Valsky, D. V.; Yagel, S.; Celnikier, D. H.; Anteby, E. Y. *Prenat. Diagn.* **2003**, *23*, 431–433.
- (19) Minuth, A. N. W.; Nottebohm, G. A.; Eknayan, G.; Suki, W. N. *Arch. Intern. Med.* **1975**, *135*, 807–810.
- (20) Smyth, J. M.; Collier, P. S.; Darwish, M.; Millership, J. S.; Halliday, H. L.; Petersen, S.; McElnay, J. C. *Br. J. Clin. Pharmacol.* **2004**, *58*, 249–258.
- (21) Chen, X.; Morris, K. R.; Griesser, U. J.; Byrn, S. R.; Stowell, J. G. *J. Am. Chem. Soc.* **2002**, *124*, 15012–15019.
- (22) Yamashita H.; Hirakura Y.; Yuda M.; Terada K. *Pharm. Res.* **2014**, *31*, 1946–1957.
- (23) Kojima T.; Tsutsumi S.; Yamamoto K.; Ikeda Y.; Moriwaki T. *Int. J. Pharm.* **2010**, *399*, 52–59.
- (24) Basavoju, S.; Boström, D.; Velaga, S. P. *Pharm. Res.* **2008**, *25*, 530–541.

- (25) Padrela, L.; Rodrigues, M. A.; Velaga, S. P.; Fernandes, A. C.; Matos, H. A.; de Azevedo, E. G. *J. Supercrit. Fluids* **2010**, *53*, 156–164.
- (26) Lin, H.; Zhang, G.; Huang, Y.; Lin, S. *J. Pharm. Sci.* **2014**, *103*, 2386–2395.
- (27) Majumder, M.; Buckton, G.; Rawlinson-Malone, C.; Williams, A. C.; Spillman, M. J.; Shankland, N.; Shankland, K. *CrystEngComm* **2011**, *13*, 6327–6328.
- (28) Umeda, Y.; Fukami, T.; Furuishi, T.; Suzuki, T.; Tanjoh, K.; Tomono, K. *Drug Dev. Ind. Pharm.* **2009**, *35*, 843–851.
- (29) Hoy, S. M.; Scott, L. J. *CNS Drugs* **2011**, *25*, 343–358.
- (30) Geppi, M.; Mollica, G.; Borsacchi, S.; Veracini, C. A. *Appl. Spectrosc. Rev.* **2008**, *43*, 202–302.
- (31) Potrzebowski, M. J. in “*NMR Crystallography*”; eMagRes; John Wiley & Sons, Ltd: Chichester, UK, **2009**, 435–453.
- (32) Alberto Monti, G.; Karina Chattah, A.; Garro Linck, Y. *Annu. Rep. NMR Spectrosc.* **2014**, *83*, 221–269.
- (33) Veinberg, S. L.; Johnston, K. E.; Jaroszewicz, M. J.; Kispal, B. M.; Mireault, C. R.; Kobayashi, T.; Pruski, M.; Schurko, R. W. *Phys. Chem. Chem. Phys.* **2016**, *18*, 17713–17730.
- (34) Apperley, D. C.; Forster, A. H.; Fournier, R.; Harris, R. K.; Hodgkinson, P.; Lancaster, R. W.; Rades, T. *Magn. Reson. Chem.* **2005**, *43*, 881–892.
- (35) Ukmar, T.; Kaucic, V.; Mali, G. *Acta Chim. Slov.* **2011**, *58*, 425–433.

- (36) Bradley, J. P.; Velaga, S. P.; Antzutkin, O. N.; Brown, S. P. *Cryst. Growth Des.* **2011**, *11*, 3463–3471.
- (37) Dudenko, D. V.; Yates, J. R.; Harris, K. D. M.; Brown, S. P. *CrystEngComm* **2013**, *15*, 8797–8807.
- (38) Maruyoshi, K.; Iuga, D.; Antzutkin, O. N.; Alhalaweh, A.; Velaga, S. P.; Brown, S. P. *Chem. Commun.* **2012**, *48*, 10844–10846.
- (39) Fahmy S.; Abu-Gharbieh E. *BioMed Res. Int.* **2014**, 590848.
- (40) Kistenmacher T. J.; Marsh R.E. *J. Am. Chem. Soc.* **1972**, *94*, 1340–1345.
- (41) Lehmann C. W.; Stowasser F. *Chem. Eur. J.* **2007**, *13*, 2908–2911.
- (42) Saalwächter K.; Lange F.; Matyjaszewski K.; Huang C.; Graf R. *J. Magn. Reson.* **2011**, *212*, 204–215.
- (43) Althaus S. M.; Mao K.; Stringer J. A.; Kobayashi T.; Pruski M. *Solid State Nucl. Magn. Reson.* **2014**, *57-58*, 17–21.
- (44) Scholz, I.; Hodgkinson, P.; Meier, B. H.; Ernst, M. *J. Chem. Phys.* **2009**, *130*, 114510.
- (45) Nielsen N. C.; Bildsoe H.; Jakobsen H. J.; Levitt M. H. *J. Chem. Phys.* **1994**, *101*, 1805–1812.
- (46) Wiench J. W.; Bronnimann C. E.; Lin V. S.; Pruski M. *J. Am. Chem. Soc.* **2007**, *129*, 12076–12077.

- (47) Lemmerer, A.; Bernstein, J.; Kahlenberg, V. *CrystEngComm* **2010**, *12*, 2856–2864.
- (48) Bis J. A.; Zaworotko M. J. *Cryst. Growth Des.* **2005**, *5*, 1169–1179.
- (49) Dudenko D. V.; Williams P. A.; Hughes C. E.; Antzutkin O. N.; Velaga S. P.; Brown S. P.; Harris K. D. M. *J. Phys. Chem. C* **2013**, *117*, 12258–12265.
- (50) Weyna D. R.; Shattock T.; Vishweshwar P.; Zaworotko M. J. *Cryst. Growth Des.* **2009**, *9*, 1106–1123.
- (51) Chierotti, M. R.; Gobetto, R. *Chem. Commun.* **2008**, 1621–1634.
- (52) Ali, H. R. H.; Alhalaweh, A.; Mendes N. F. C.; Ribeiro-Claro P.; Velaga S. P. *CrystEngComm* **2012**, *14*, 6665–6674.
- (53) Desiraju G. R.; Steiner T. in “*The Weak Hydrogen Bond In Structural Chemistry and Biology*”, Eds. Oxford University Press, New York, **2006**.
- (54) Martinez, C. R.; Iverson, B. L. *Chem. Sci.* **2012**, *3*, 2191–2201.
- (55) Gobetto, R.; Nervi, C.; Chierotti, M. R.; Braga, D.; Maini, L.; Grepioni, F.; Harris, R. K.; Hodgkinson, P. **2005**, *11*, 7461–7471.
- (56) Nishiyama Y.; Endo Y.; Nemoto T.; Utsumi H.; Yamauchi K.; Hioka K.; Asakura T. *J. Magn. Reson.* **2011**, *208*, 44–48.
- (57) Pandey M. K.; Amoureux J.; Asakura T.; Nishiyama Y. *Phys. Chem. Chem. Phys.* **2016**, *18*, 22583–22589.
- (58) Schmidt, J.; Hoffmann, A.; Spiess, H. W.; Sebastiani, D. *J. Phys. Chem. B* **2006**, *110*, 23204–23210.



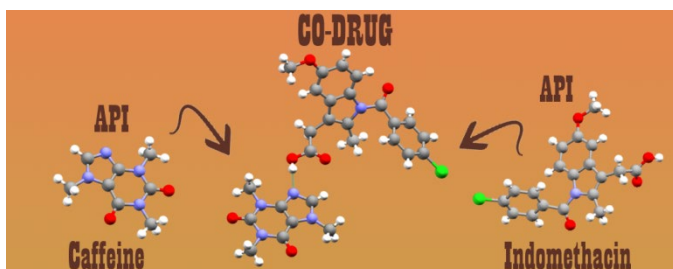
(59) Savjani K. T.; Gajjar A. K.; Savjani J. K. *ISRN Pharm.* **2012**, 195727.

## For Table of Contents Use Only

### Engineering co-drug solid forms: the mechanochemical synthesis of an indomethacin-caffeine system

Simone Bordignon, Paolo Cerreia Vioglio, Emanuele Priola, Dario Voinovich, Roberto Gobetto, Yusuke Nishiyama and Michele R. Chierotti

#### TOC



#### SYNOPSIS

We report on the preparation and solid-state characterization of a drug-drug cocrystal between indomethacin and caffeine in a 1:1 stoichiometry. Characterization consisted in a combination of PXRD and SCXRD analyses, vibrational spectroscopies and solid-state NMR measurements, calorimetric measurements and dissolution kinetic tests (DKT). The latter revealed superior bioavailability of indomethacin in the cocrystal compared to pure indomethacin.